



Elimination of pores in Ag–Sn TLP bonds by the introduction of dissimilar intermetallic phases

Huakai Shao^{1,*}, Aiping Wu^{1,2,3}, Yudian Bao¹, and Yue Zhao^{1,3}

¹Department of Mechanical Engineering, Tsinghua University, Beijing 100084, China

²State Key Laboratory of Tribology, Tsinghua University, Beijing 100084, China

³Key Laboratory for Advanced Materials Processing Technology, Ministry of Education, Beijing 100084, China

Received: 22 July 2016

Accepted: 25 November 2016

Published online:

5 December 2016

© Springer Science+Business Media New York 2016

ABSTRACT

Low-temperature transient liquid phase (TLP) bonding is a very promising technology for achieving die attachment in high-temperature power devices. However, the Ag–Sn TLP-bonded joint has high sensitivity to shrinkage pores, which will lead to the deterioration of mechanical, thermal, and electrical properties. In this study, we have proposed two novel methods to solve the problem of pores in Ag–Sn TLP bonding through the introduction of second phases. The first method is replacing Ag substrate on one side with Cu substrate to create dual layers of dissimilar intermetallic compounds (IMCs). Consequently, the dual layers of Cu_6Sn_5 (or Cu_3Sn) and Ag_3Sn IMCs emerge on the cross-sections of bonded joint, resulting in the effective elimination of pores, which can be attributed to the change of the microstructure and the interface migration between two dissimilar IMC layers (e.g., $\text{Cu}_6\text{Sn}_5/\text{Ag}_3\text{Sn}$). The second method is coating a thin Cu film on the Ag substrate to introduce Cu–Sn IMC particles. As a result, a great number of Cu_6Sn_5 particles disperse in the middle of the Ag_3Sn layer, filling the micropores efficiently, such that a significant decrease in shrinkage pores is achieved. Both methods have been experimentally verified to improve the mechanical properties, and they have high potential to be implemented in other TLP systems.

Introduction

Low-temperature transient liquid phase (TLP) bonding is an extremely promising technology for achieving die attachment in high-temperature power devices, particularly wide-band gap semiconductors such as silicon carbide (SiC) and gallium nitride, which are widely employed in the automotive,

aerospace, deep-well drilling, and energy production industries [1, 2]. This approach ensures that devices can be operated at high temperatures without failure, because TLP joints are generally composed of full intermetallic compounds (IMCs), which have much higher remelting points in comparison to the temperatures in the bonding process ($<300\text{ }^\circ\text{C}$) [3]. In recent years, many researchers have made

Address correspondence to E-mail: shk13@mails.tsinghua.edu.cn

considerable progress by focusing on the growth mechanisms, morphological characterizations, and mechanical properties of IMCs from different systems, such as Cu–Sn [4], Ni–Sn [5], Au–Sn [6], Ag–Sn [7], and Cu–In [8]. The literatures report that pore defects form easily in TLP joints [9–12], which may severely reduce their reliability in terms of electrical conductivity and mechanical properties.

Three types of void exist, defined according to their formation processes and characteristics: the Kirkendall void, processing pore, and shrinkage pore. Kirkendall voids are initiated by unbalanced diffusions of different elements at the interface; they are especially common in the Cu–Sn TLP system, in which the voids are usually located along the Cu/Cu₃Sn interface [12]. In general, the formation of Kirkendall voids is supposed to result from impurities like sulfur that are incorporated during electroplating [13]. However, the latest study suggests that the grain size of the substrate is a principal factor, and fine-grained base materials induce more Kirkendall voids because of the increase in diffusion paths of the grain boundary [14]. It is reported that heat treatment on the metallization layer can significantly reduce the incidence of Kirkendall voids [15], because heat treatment reduces the content of impurity elements and suppresses their segregation [16]. Furthermore, coarsened grains can decrease the grain boundaries for diffusion as well [14].

Bosco et al. [9] first paid attention to the distribution of pores along the central zone of the IMC joints. They proposed that these pores form prior to the occurrence of the liquid phase, as most of the deposited interlayer is consumed during solid-state reactions, and the liquid is not sufficient to successfully accomplish TLP bonding at the targeted temperature. This kind of defect is called a processing pore because of its formation process. Processing pores tend to be generated in situations with deposited interlayers, like electroplated Sn [9, 10]. However, researchers have identified a critical thickness of interlayer that can produce pore-free joints, which is strongly associated with the heating rate. Two methods have been suggested for avoiding this type of pore. Wang et al. [9] found that annealing the substrate to coarsen the grains can improve the mechanical integrity of Ag–In TLP joints, since the decreased grain boundaries restrain solid-state diffusions. It has also been reported that the insertion of a buffer layer of an element like Ni between the

substrate and the deposited interlayer can suppress atom diffusions in the solid state [17–19].

Shrinkage pores represent a very familiar defect in Ag–Sn [11] and Ni–Sn [20] TLP joints. They are generally located in the middle of the IMC layer, where the final molten Sn islands are consumed. The formation of a shrinkage pore occurs as a consequence of volume shrinkage during isothermal solidification. Some researchers have investigated the characteristics of shrinkage pores, but no effective solutions have yet been proposed to reduce or eliminate them. This paper systematically investigates the elimination of shrinkage pores through two novel approaches: the formation of dual layers of dissimilar IMCs (e.g. Cu₆Sn₅/Ag₃Sn or Cu₃Sn/Ag₃Sn) and the introduction of second-phase particles. Both modified methods can produce largely pore-free joints.

Experimental procedure

Two polished pure Cu (99.9%) rods with the dimension of 10 and 6 mm diameter and 5.5 mm length were electroplated with 25- μ m-thick Ag layer, to be used as the substrate. Commercially available pure Sn (99.9%) foil with 10 μ m thickness was utilized as the solder interlayer. Prior to bonding process, the Ag-plated substrate was ultrasonically cleaned in 5 vol% HNO₃ solution for 5 min, followed by rinsing with deionized water and anhydrous alcohol, and dried at last. The Sn foil was firstly dipped in acetone for several minutes and then washed with anhydrous alcohol. After being mildly coated with resin flux, the Sn foil was inserted into the two different substrates. A preliminary experiment was conducted to investigate the Ag/Sn/Ag sandwich TLP bonding. However, our previous study indicated that a large amount of pores formed in the middle of the IMC layer [21].

In order to avoid unnecessary impacts from residual flux and clearly observe the appearance of the pores, another preliminary experiment was performed using 25- μ m-thick Sn foil under vacuum condition. Figure 1 shows the cross-sectional microstructures of the Ag/Sn/Ag TLP joints. Many large pores started to form alongside the Sn islands just as Ag₃Sn scallops on both sides contacted with each other (Fig. 1a). Their sizes significantly increased after the molten Sn was completely consumed (Fig. 1b). This change suggests that the

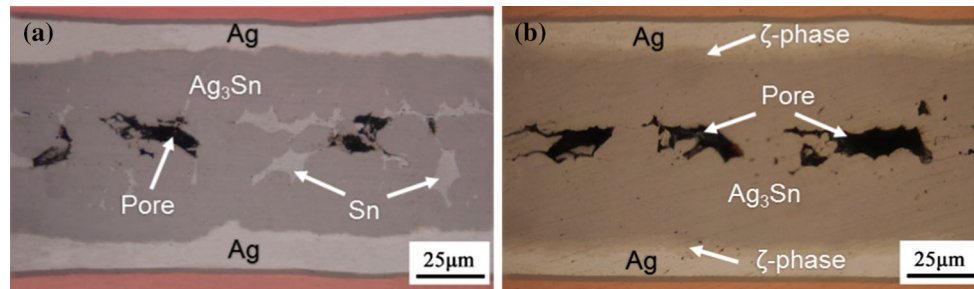


Figure 1 Characterizations of the pores in Ag–Sn TLP joints formed at 280 °C for **a** 150 min (containing Sn islands) and **b** 300 min (composed of full IMCs), where the bonding pressure is about 0.2 MPa.

formation of pores is attributed to volume shrinkage of the liquid Sn islands during isothermal solidification.

However, if a second intermetallic phase is introduced to change the microstructure or fill the pores, it is believed that these defects will be effectively eliminated. Two modified methods were proposed to prevent pore formation in TLP joints. In the first one, the bottom Ag-plated substrate was substituted by a pure Cu rod to produce dual layers of dissimilar IMCs, as depicted in Fig. 2a. In the other one, a thin Cu film with thickness being varied among 0.5, 1.5, and 3.0 μm was electroplated on the upper Ag-plated substrate, so as to bring Cu–Sn IMCs in the Ag_3Sn layer, as depicted in Fig. 2b. After cleaning, the sandwich samples fabricated by the modified methods were placed into a resistance furnace.

The joining experiment was carried out in air atmosphere. The bonding pressure of 0.3 MPa was applied by the weight of stainless steel block. A heating rate of 10 °C/min was selected but a slow cooling rate of approximately 2–3 °C/min was employed. The bonding temperatures were among 250, 300, and 350 °C. The bonding time was determined by the thickness of the interlayer, within the range of 60–420 min. After finishing the TLP processes, the bonded samples were mounted in epoxy resin, then successively ground by 240, 600, 1000, 1500, and 2000 grade SiC papers, and eventually polished using diamond polishing agents. The microstructures were investigated by optical microscopy, scanning electron microscopy (SEM), energy-dispersive X-ray spectroscopy (EDS), and electron probe microanalysis (EPMA). In order to evaluate the mechanical properties of the TLP joints produced by the modified approaches, shear test was conducted on a Gleeble 1500D thermal simulated test machine with a shear rate of 2 mm/min. At least five

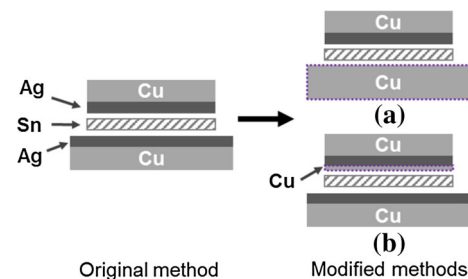


Figure 2 Schematic of the sandwich samples for bonding process. **a** Replacing Ag-plated substrate on one side with Cu substrate and **b** coating a thin Cu film on the Ag-plated substrate.

specimens were adopted to determine the shear strength under the same testing condition.

Results and discussion

Defect elimination through Cu/Sn/Ag TLP bonding

TLP bonding on the Cu/Sn/Ag sandwich samples was performed at different temperatures, and the microstructures were observed under SEM. In a previous study, we demonstrated that no ternary alloy phases were generated in the Cu/Sn/Ag TLP joints when the bonding temperatures were lower than 350 °C [22], and another study obtained similar conclusions [23]. Based on the binary phase diagrams of Cu–Sn and Ag–Sn systems [24] and the backscattered electron images, the corresponding layers of IMCs were labeled as Ag_3Sn , ζ -phase, Cu_6Sn_5 , and Cu_3Sn , as shown in Fig. 3. The images demonstrate that all of the Cu/Sn/Ag bonded samples obtained at different temperatures contained many fewer micropores than the Ag/Sn/Ag TLP joints.

In the 250 °C bonded sample, a few pores remained along the $\text{Cu}_6\text{Sn}_5/\text{Ag}_3\text{Sn}$ interface after

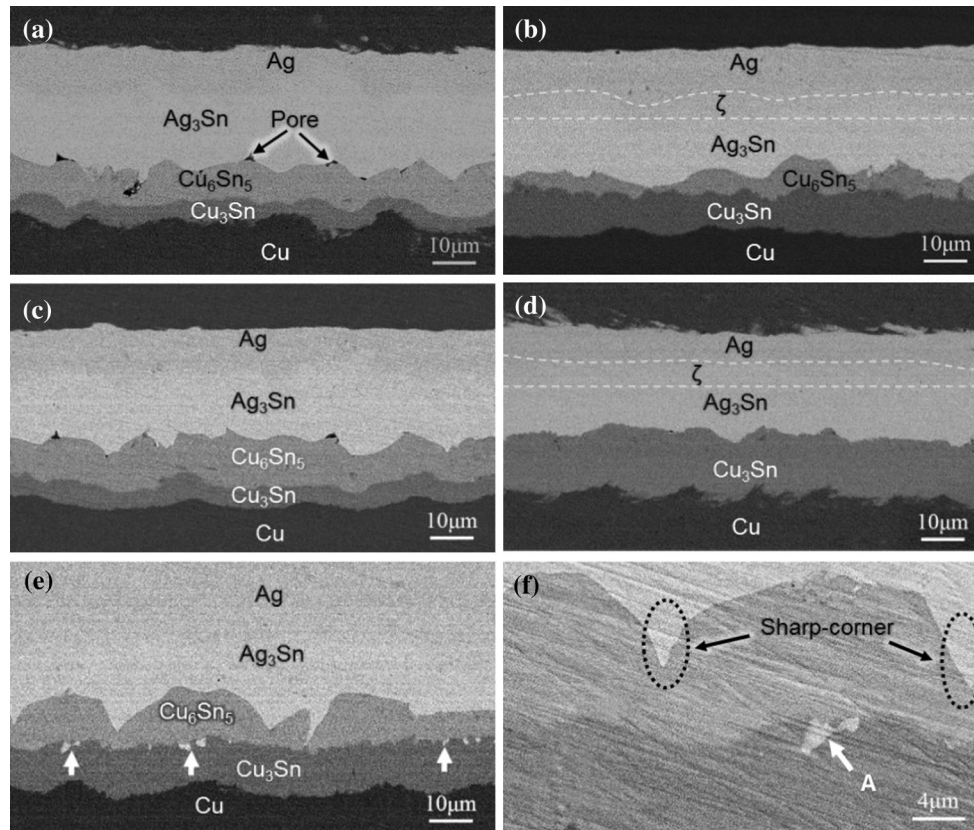


Figure 3 Cross-sectional microstructures of the Cu/Sn/Ag TLP joints formed at **a** 250 °C for 240 min, **b** 250 °C for 420 min, **c** 300 °C for 90 min, **d** 300 °C for 420 min, and **e** 350 °C for 60 min and **f** magnification of the area marked by *arrow marks*.

processing for a short period of time (Fig. 3a); they were particularly concentrated adjacent to the side of the Ag_3Sn layer and between neighboring Ag_3Sn grains. However, no pores remained in the joint when the bonding time was prolonged to 420 min (Fig. 3b), although the microstructure was otherwise similar to that produced by the TLP process with a bonding time of over 240 min. A wave-shaped interface emerged between the Cu_6Sn_5 and Ag_3Sn layers, becoming more planar with relatively long homogenization. This phenomenon indicates that interface migration occurred between the Cu_6Sn_5 and Ag_3Sn layers, leading to the elimination of pores.

In the samples bonded at 300 °C, a significant reduction in defect size and quantity was observed in the joint after bonding for 90 min (Fig. 3c). However, pores no longer appeared when the bonding time increased to 420 min (Fig. 3d), and the Cu_6Sn_5 completely transformed into Cu_3Sn IMCs. Interestingly, the wave-shaped interface between the Cu_6Sn_5 and Ag_3Sn layers was converted into a nearly planar $\text{Cu}_3\text{Sn}/\text{Ag}_3\text{Sn}$ interface during this process. This

finding reveals that interface migration might have taken place as scalloped Cu_6Sn_5 evolved into columnar Cu_3Sn grains (the morphology of Cu_3Sn grain is described in previous studies [4, 25]).

When bonding occurred at 350 °C, no noticeable pores were observed at the $\text{Cu}_6\text{Sn}_5/\text{Ag}_3\text{Sn}$ interface, and the wave shape of the $\text{Cu}_6\text{Sn}_5/\text{Ag}_3\text{Sn}$ interface approximated a zigzag pattern (Fig. 3e). Furthermore, many bright microparticles, identified as Ag_3Sn by EDS analysis (atomic percentage of Cu:Ag:Sn = 6.92:70.15:22.93 for the arrowed A), were distributed along the $\text{Cu}_6\text{Sn}_5/\text{Cu}_3\text{Sn}$ interface. In fact, the amplified SEM image indicates that these Ag_3Sn particles were closer to the Cu_3Sn layer but not in the Cu_6Sn_5 layer (Fig. 3f). The Ag atoms appeared to diffuse along the grooves between two neighboring Cu_6Sn_5 grains at early stages, reaching the $\text{Cu}_6\text{Sn}_5/\text{Cu}_3\text{Sn}$ interface at a relatively higher bonding temperature. Additionally, Sn atoms diffused rapidly across the Cu_6Sn_5 scallops, even more quickly than Cu atoms [26]. In this way, Ag_3Sn grains nucleated and coarsened at the interface, resulting in the

formation of microparticles. However, the $\text{Cu}_6\text{Sn}_5/\text{Cu}_3\text{Sn}$ interface migrated toward the Cu_6Sn_5 layer due to phase transition from Cu_6Sn_5 to Cu_3Sn , seemingly “entrapping” Ag_3Sn particles in the Cu_3Sn layer. In addition, some sharp Ag_3Sn corners fell in the Cu_6Sn_5 grain boundaries (Fig. 3f), where pores theoretically should have been more inclined to form. However, no defects were found at the top of the sharp Ag_3Sn corners, suggesting rapid interface migration at higher temperatures.

The above analysis suggests that the elimination of pores in this method can be attributed to two factors. On the one hand, the formation of Cu–Sn IMCs on the opposite side of the Ag_3Sn layer changes the joint microstructure, significantly reducing the size and quantity of pores after full consumption of Sn, as shown in Fig. 3a, c. On the other hand, interface migration between Cu–Sn IMCs and Ag_3Sn layers occurs during homogenization, further eliminating pores in the joint, as shown in Fig. 3b, d.

However, questions remain as to why the interface of dissimilar IMCs migrates, or why wave-shaped interfaces become more planar during homogenization. The Gibbs free energy of the interface provides answers, and it can be found as follows:

$$G = \sigma A, \quad (1)$$

where σ is the interface energy of the IMCs, which is equal to the interface tension in numerical value [27], and A is the area of the interface. If Ag_3Sn and Cu–Sn IMC grains could merge and ripen into a new, larger grain of ternary alloy phase across the entire joint, like in the Cu/Sn/Cu TLP reaction [4], a reduction in Gibbs free energy would be achieved by the phase transition. However, this is not possible, because the independent interface always exists. Therefore, the change in interface curvature is the force that lowers the Gibbs free energy. In Eq. 1, when the value of A reaches its minimum, the Gibbs free energy of the interface is at its lowest point. Therefore, the wave-shaped interface of dissimilar IMCs inevitably becomes more planar in order to reduce the interface area in the subsequent homogenization.

Based on the previous studies [28, 29], this study proposes that the driving force is the interface curvature. The migration rate of the interface movement can be described as follows [28]:

$$M = p \frac{bv\Omega}{kT} e^{-\frac{\Delta G}{kT}}, \quad (2)$$

where p is the driving force related to the interface curvature, b is the interface displacement associated with the thermally activated hopping of single atoms, v is the Debye frequency, ΔG is the difference in free energies between the atoms in the two IMCs, T is the temperature, k is the Boltzmann constant, and Ω is the volume associated with the hopping atom. According to this equation, the migration rate increases with the increase in interface curvature (p) and bonding temperature (T). This can be used to explain the remarkable decrease in pores at higher temperatures, especially in terms of the abnormal phenomenon depicted in Fig. 3f.

The method by which interface migration proceeds is another point of interest. Figure 4 shows the elemental distributions of Cu, Sn, and Ag in the Cu/Sn/Ag TLP joint, in which a few Cu_6Sn_5 islands remained between the Ag_3Sn and Cu_3Sn layers. A noticeable boundary exists in the Cu and Ag elemental distribution, and no Cu or Ag atoms can be detected on the sides of the Ag_3Sn or Cu–Sn IMC layers. In other words, no significant interdiffusions occurred between the Ag_3Sn and Cu–Sn IMC layers. Therefore, we suggest that self-diffusions on both sides of the interface of dissimilar IMCs were primarily responsible for controlling the interface migration and filling the pores.

Some typical cross-sections of the Cu/Sn/Ag TLP joint were treated by ion-beam milling in order to observe clearly the dissimilar IMC interfaces, as shown in Fig. 5. Interestingly, the wave-shaped $\text{Cu}_6\text{Sn}_5/\text{Ag}_3\text{Sn}$ interface presents a smooth morphology, while the planar $\text{Cu}_3\text{Sn}/\text{Ag}_3\text{Sn}$ interface exhibits relatively rough features. We attribute this difference to the morphological characterizations of the Cu_6Sn_5 and Cu_3Sn grains, which take the forms of scalloped and columnar crystals, respectively [4], and may affect the cohesion strength of the interface. In fact, the different grain morphologies probably affect the combination pattern between Ag_3Sn and Cu–Sn IMCs, and the facets of the Cu_3Sn grains may induce the formation of the planar $\text{Cu}_3\text{Sn}/\text{Ag}_3\text{Sn}$ interface.

Defect elimination through Ag(Cu)/Sn/Ag TLP bonding

TLP bonding at different temperatures and various time durations was carried out for samples in which the Ag substrate was coated with a 1.5- μm -thick Cu

Figure 4 EPMA mapping images of the Cu/Sn/Ag TLP joint formed at 300 °C for 300 min.

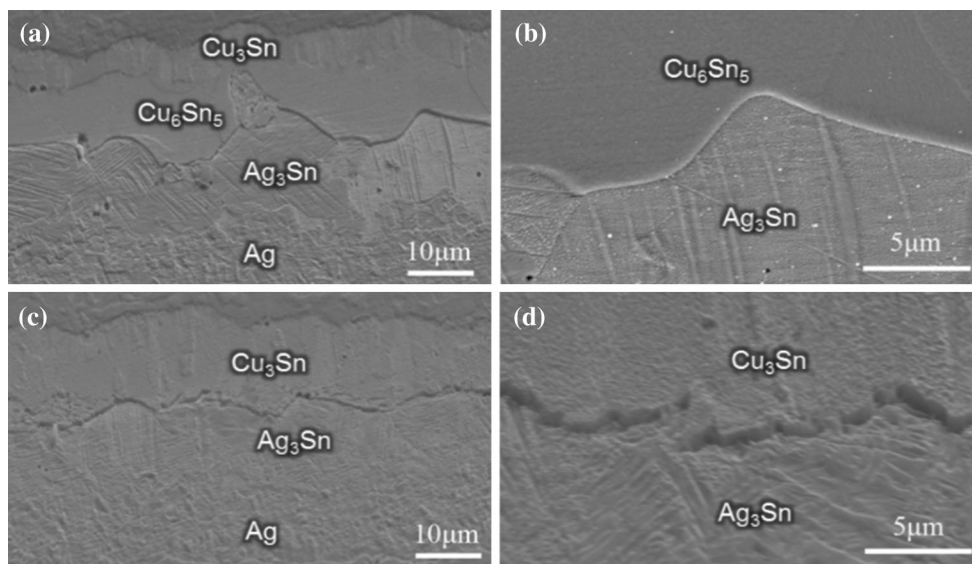
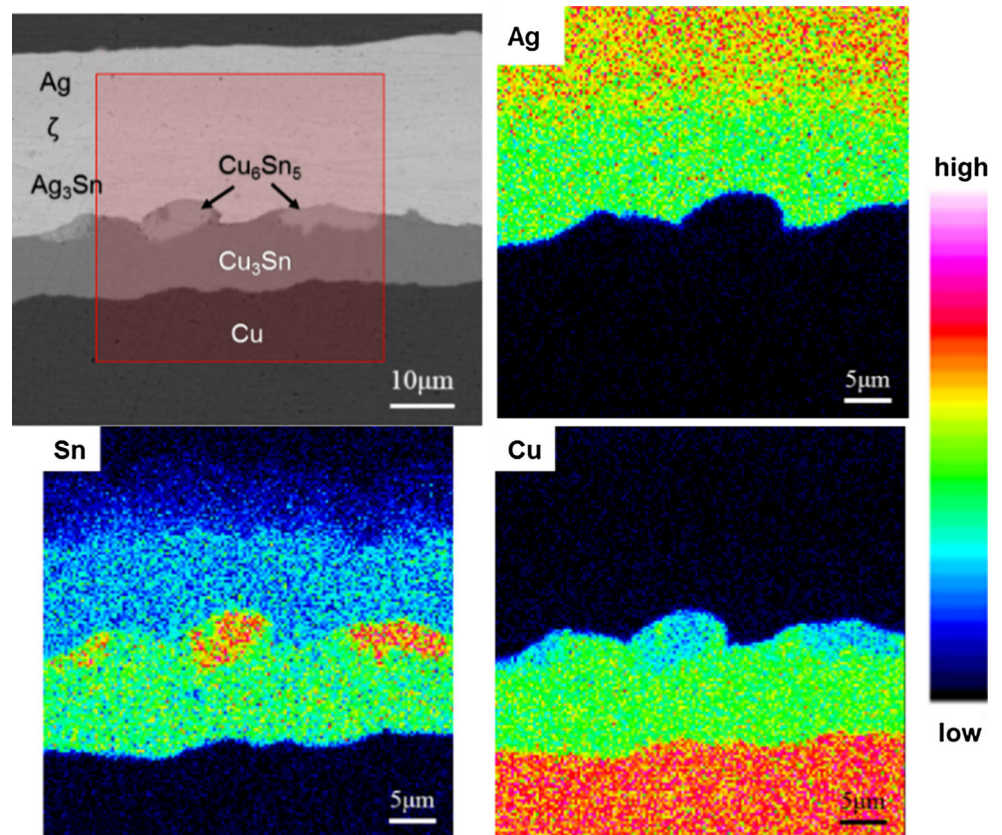


Figure 5 Topographic characterizations of the a, b $\text{Cu}_6\text{Sn}_5/\text{Ag}_3\text{Sn}$ interface and c, d $\text{Cu}_3\text{Sn}/\text{Ag}_3\text{Sn}$ interface.

film. The joint produced by bonding at 300 °C for 90 min (Fig. 6a) contained many spherical and irregularly shaped particles that were dispersed in the middle of the Ag_3Sn layer and filled micropores. EDS analysis identified these embedded particles as

Cu–Sn IMCs (atomic percentage of Cu:Sn = 63.54:36.46 for the arrowed B). Figure 6b clearly shows a typical IMC particle, which is primarily composed of a large-sized Cu_6Sn_5 core (light area) partially covered by a thin Cu_3Sn shell (dark area). We propose that this structure

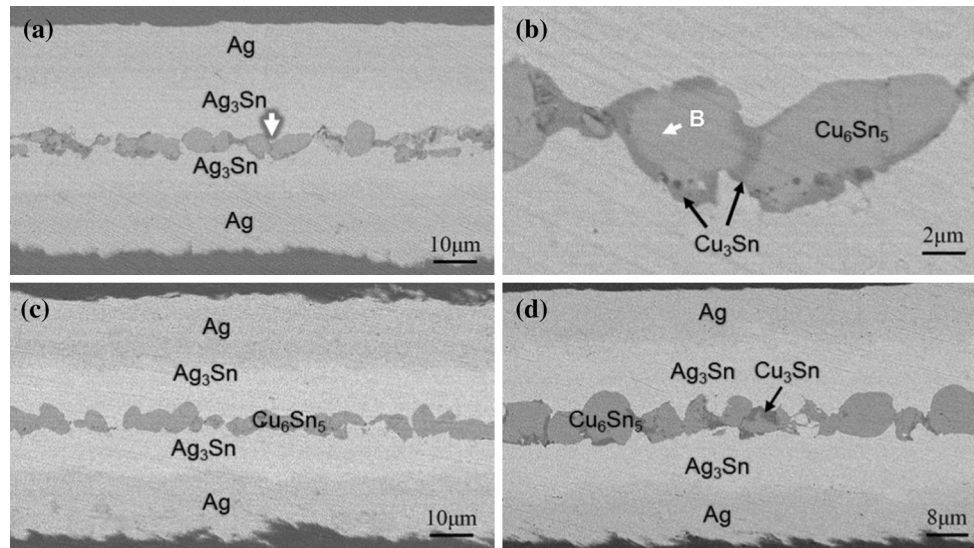


Figure 6 Cross-sectional microstructures of the Ag(Cu)/Sn/Ag TLP joints formed at **a** 300 °C for 90 min, **b** magnification of the area marked with the *black arrow mark*, **c** 250 °C for 240 min, and **d** 350 °C for 60 min, where the thickness of the Cu film is 1.5 μm .

resulted from the formation of an ultra-thin Cu_3Sn layer between the Cu film and Cu_6Sn_5 scallops during a Cu/Sn solid–liquid reaction, followed by the detachment of the Cu–Sn IMCs from the Ag-plated substrate after the total consumption of the Cu film.

The microstructures of the joints formed at 250 °C (Fig. 6c) and 350 °C (Fig. 6d) are quite similar. However, only Cu_6Sn_5 IMCs were identified in the 250 °C bonded sample, while a thicker Cu_3Sn shell was detected in the 350 °C bonded sample. This phenomenon may be attributed to the higher growth rate of Cu_3Sn IMCs at higher bonding temperatures. Even so, the different particle sizes and shapes can perfectly fill the micropores in the different bonded samples. Therefore, we propose that the elimination of pores in this method generally depends on the quantity of second-phase particles, but not their sizes or shapes, because this study detected no abnormal growth of Cu–Sn IMC particles.

This study also investigated the influence of the thickness of the Cu film on the microstructure under bonding at 300 °C for 90 min. In the 0.5- μm -thick Cu film bonded sample (Fig. 7a), only a small amount of Cu_6Sn_5 particles formed, insufficient to fill the pores completely, such that many pores remained along the Ag_3Sn grain boundaries. However, when the Cu film was very thick, about 3.0 μm (Fig. 7b), continuously layered Cu_6Sn_5 IMCs appeared between two different Ag_3Sn layers, accompanied by the disappearance of pores. Therefore, we can conclude that the Ag–Sn

TLP process cannot fully eliminate pores in the presence of an excessively thin layer of Cu film, while layered Cu_6Sn_5 will always maintain its band-like distribution instead of a typical particle dispersion in a process with an excessively thick Cu film.

Figure 7c, d shows the morphologies of Cu_6Sn_5 particles alongside the Ag_3Sn scallops, in which the residual Sn was slightly etched. The Ag_3Sn layer on the upper Ag substrate is remarkably thinner than that on the bottom Ag substrate, due to the buffer effect of the Cu film in the Ag/Sn early-stage reaction. The Cu_6Sn_5 particles are not only located in the residual Sn, but are also attached to the Ag_3Sn grains. In addition, some Cu_6Sn_5 particles began to detach from the Ag_3Sn layer at this time, as highlighted by the arrows, where the root of the Cu_6Sn_5 grains necked down. Since no more Cu flux could be supplied, the Ag_3Sn grains pushed them toward the centerline of the liquid phase. Moreover, the number of Cu_6Sn_5 particles significantly increased as the Cu film thickness increased from 0.5 to 1.5 μm . These results indicate that the thickness of the Cu film plays a very important role in the elimination of pores in this method.

The formation of Cu_6Sn_5 particles may affect the growth kinetics of the Ag_3Sn layer [30], but it cannot change the scalloped shape of the Ag_3Sn grains. Other studies proposed that the filling effect of Cu_6Sn_5 particles on the micropores mainly governs the elimination of pores in this method [30, 31]. In this

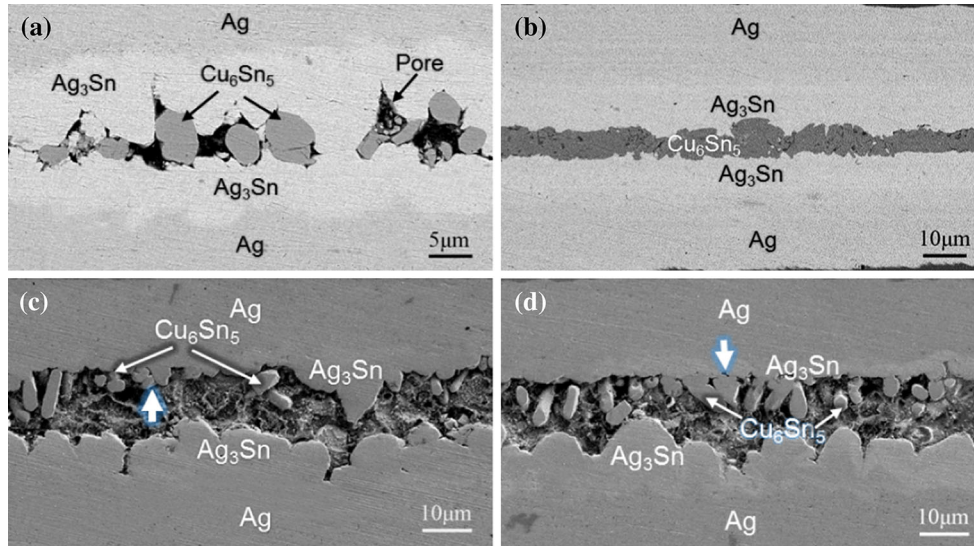


Figure 7 Cross-sectional microstructures of the Ag(Cu)/Sn/Ag TLP joints formed at 300 °C for 90 min with **a** 0.5-μm and **b** 3.0-μm Cu film, and at 300 °C for 5 min with **c** 0.5-μm and **d** 1.5-μm Cu film.

study, a critical thickness of Cu film was proposed to establish different reaction models for Ag(Cu)/Sn/Ag TLP bonding with different distribution shapes of Cu–Sn IMCs. In detail, if the thickness of Cu film is less than the critical value (Fig. 8a), the thin Cu film rapidly transforms into Cu₆Sn₅ particles, which dissolve into molten Sn within a short period of time; as the reaction continues, the Cu₆Sn₅ particles are pushed toward the centerline of the liquid phase by the growing Ag₃Sn scallops, until they finally disperse in the middle of the Ag₃Sn layer. However, if the thickness of the Cu film is greater than the critical value (Fig. 8b), scalloped Cu₆Sn₅ grains grow directly on the Cu film, thickening along the normal direction of the substrate until the Cu₆Sn₅ layer impinges on the opposite Ag₃Sn layer; pores can be eliminated by interface migration during the homogenization process, like in the Cu/Sn/Ag reaction, and the Cu film may or may not remain. If liquid still remains after the Cu film is fully consumed, Ag₃Sn is probably generated between the Cu₆Sn₅ layer and the Ag substrate coated with Cu film, because Sn atoms can diffuse across the Cu₆Sn₅ layer and react with Ag. This process is shown in Fig. 7b.

We propose that the critical thickness of the Cu film is related to its dissolution in liquid Sn, in particular during the early solid–liquid reaction stage. In fact, the dissolution process of the material can be expressed by Dybkov’s equation [32]:

$$\frac{dC}{dt} = k \frac{S}{V} (C_S - C), \tag{3}$$

where k is the dissolution rate constant, S is the surface area of the substrate contacting with the molten solder, V is the volume of the molten solder, C_S is the equilibrium concentration of the substrate element in the molten solder (solubility), and C is the concentration of the substrate element at time t . The value of C_S can be obtained from the equilibrium phase diagram, and it is a constant for a given temperature. As Eq. 3 indicates, the dissolution rate of Cu film mainly depends on the real-time concentration of Cu atoms in liquid Sn (C). However, the value of C is variable because of the Cu/Sn reaction, creating a dynamic process of Cu film dissolution. Otherwise, if we consider the dissolution as a static process, we obtain the following calculation:

$$t_{Cu} = \frac{\rho_{Sn} C_S}{(1 - C_S) \rho_{Cu}} t_{Sn}, \tag{4}$$

where ρ_{Cu} and ρ_{Sn} are the densities of Cu and Sn, at 8.9 and 7.28 g/cm³, respectively; t_{Sn} is the thickness of Sn foil, at 10 μm; and the maximum solubility of Cu in molten Sn (C_S) is adopted as a reference, for example 2.9% at 300 °C [24]. Only 0.24-μm-thick Cu film could be compatible with this equation, far less than the value of 1.5 μm used in our study. This value is also not in agreement with Yoon et al. [33], who used an Ag layer approximately 4 μm thick; in their study, the Ag film completely dissolved in the molten SAC solder at

Figure 8 Reaction models of the Ag(Cu)/Sn/Ag TLP process determined by the thickness of the actually coated Cu film. **a** Less than and **b** greater than the critical thickness of the Cu film.

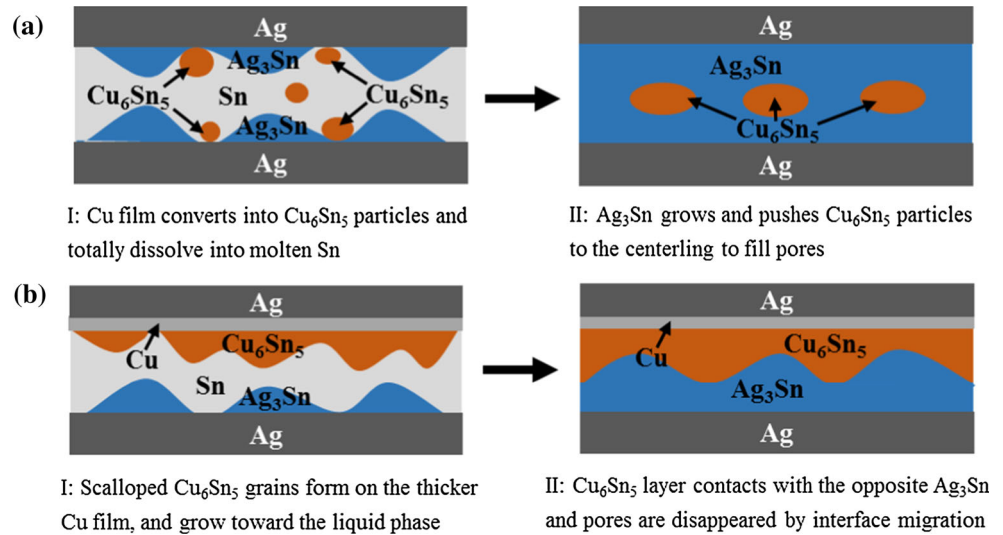
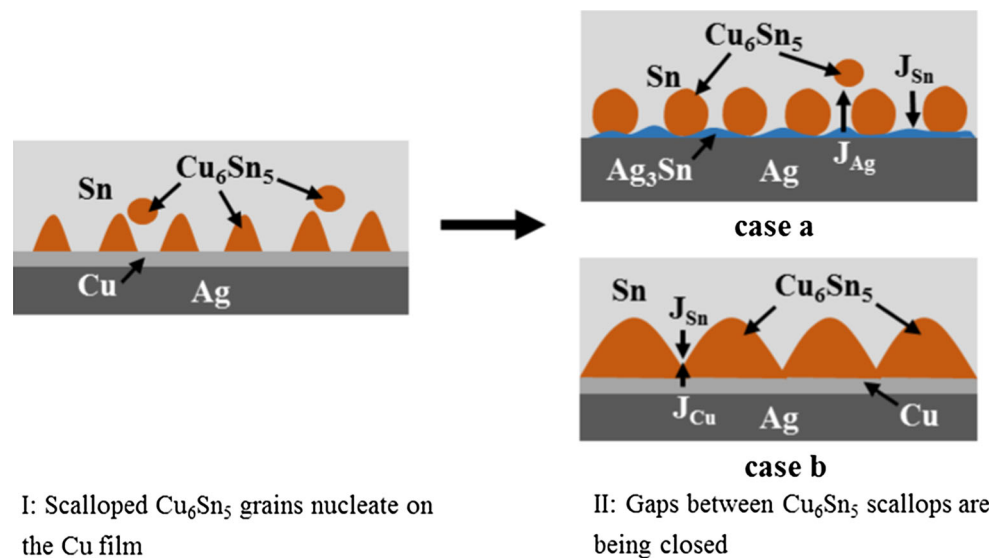


Figure 9 Growth model of the Cu_6Sn_5 grains in early Ag(Cu)/Sn reaction. *Case A* indicates that the thickness of the Cu film is less than the critical thickness, while that in *case B* is greater than the critical thickness.



250 °C for 60 s. Therefore, the dynamic process caused by the variable C must be taken into consideration in order to estimate the critical thickness.

Building on the initial growth process of Cu_6Sn_5 grains [34], we developed a schematic model of the early Ag(Cu)/Sn reaction in order to determine the critical thickness, as illustrated in Fig. 9. This model suggests that the critical thickness can be determined based on the closed gaps between two neighboring Cu_6Sn_5 scallops. Specifically, the Cu film is totally consumed just as most of the gaps between the Cu_6Sn_5 grains close up. Therefore, the corresponding thickness of the Cu film is the critical value. In case A,

the Cu film thickness is less than the critical value; in that situation, the Cu_6Sn_5 grains neck down and detach from the Ag-plated substrate due to the full consumption of the Cu film and the nucleation of Ag_3Sn grains, creating the particle shape of the Cu–Sn IMC distribution. The spalling of Cu_6Sn_5 grains is consistently observed in the thin-film case reaction after the Cu film is consumed [35]. In case B, the Cu film thickness is greater than the critical value; the amount of Cu film allows all gaps between two neighboring Cu_6Sn_5 grains to be closed, and Cu or Sn atoms mainly diffuse along the grain boundaries to continue the reaction.

Mechanical properties of the modified TLP joint

The elimination of pores can noticeably improve the mechanical integrity and properties of TLP joints. Figure 10 shows the shear strengths of Ag/Sn/Ag, Cu/Sn/Ag, and Ag(Cu)/Sn/Ag TLP joints, where “Cu/Sn/Ag-420” indicates that the corresponding sample was bonded for 420 min. As the data demonstrate, the shear strength values of “Cu/Sn/Ag” are generally higher than those of “Ag/Sn/Ag”, except for the sample bonded at 250 °C, because some pores remain in the IMCs after short periods of homogenization. However, the value for 250 °C increases with prolonged bonding time and exceeds that of “Ag/Sn/Ag”, a result that is in agreement with the change in microstructure. Furthermore, the shear strength of the Cu/Sn/Ag TLP joint produced at 300 °C also increases with prolonged bonding time, due to further reductions in pores and the combination of Cu₃Sn and Ag₃Sn layers. This indicates that the cohesion strength between Cu₃Sn and Ag₃Sn is higher than that between Cu₆Sn₅ and Ag₃Sn. The shear strengths of “Ag(Cu)/Sn/Ag” are higher

than those of “Ag/Sn/Ag” joints, but slightly lower than those of “Cu/Sn/Ag”.

Figure 11 shows the detailed morphologies of several typical fracture surfaces. For the Cu/Sn/Ag TLP joint, cleavage steps of Ag₃Sn (atomic percentage of Ag:Sn = 75.36:24.64), smooth facets of Cu₆Sn₅ (atomic percentage of Cu:Sn = 53.12:46.88), and rough rock candies of Cu₃Sn (atomic percentage of Cu:Sn = 74.49:25.51) occur simultaneously on the Cu-side fracture surface (Fig. 11a). For the Ag(Cu)/Sn/Ag TLP joint, both shear bands of Ag₃Sn (atomic percentage of Cu:Ag:Sn = 3.12:73.56:23.32) and brittle Cu–Sn IMCs (atomic percentage of Cu:Ag:Sn = 53.76:8.81:37.43) are detected by SEM observation and EDS analysis (Fig. 11b). The microstructures obtained by the two novel methods are relatively compact according to the fracture surfaces, indicating that using the “Cu/Sn/Ag” or “Ag(Cu)/Sn/Ag” modified sandwich to interconnect the chips can indeed improve the mechanical integrity.

In summary, the two novel methods have been experimentally verified to solve the problem of pores

Figure 10 Variations in joint shear strengths with bonding temperature, where the “Cu/Sn/Ag-420” indicates that the bonding time is prolonged to 420 min.

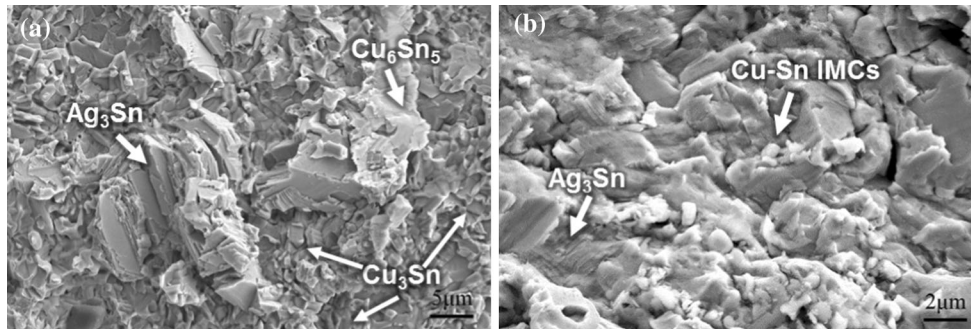
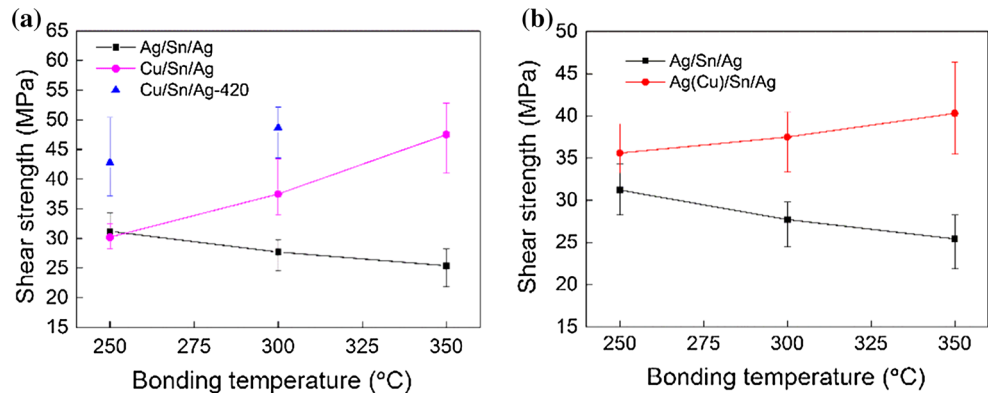


Figure 11 Fracture surfaces of the different typical joints for **a** Cu/Sn/Ag bonded at 300 °C for 300 min and **b** Ag(Cu)/Sn/Ag bonded at 300 °C for 90 min.

in Ag–Sn TLP bonding by the formation of Cu–Sn IMCs. It is suggested that the introduction of dissimilar IMCs can be helpful to other TLP systems as well, such as Ni–Sn, but the second high-temperature metal (e.g. Cu) must not react with the first high-temperature metal (e.g. Ag) to form ternary alloy phases. Chuang et al. [30] found that the formation of Ag_3Sn particles could eliminate micropores in Ni–Sn IMCs during aging treatment. Similarly, Lis et al. [11] found that dual layers of Ag_3Sn and Ni_3Sn_4 IMCs could reduce the pore formation in Ni–Sn TLP joints.

Conclusions

This paper systematically investigates the elimination of shrinkage pores in Ag–Sn TLP joints by the introduction of Cu–Sn intermetallic phases. The following conclusions can be obtained:

- (1) Replacing Ag substrate on one side with Cu substrate to create dual layers of dissimilar IMCs like $\text{Cu}_6\text{Sn}_5/\text{Ag}_3\text{Sn}$ can effectively eliminate shrinkage pores in the Ag–Sn TLP joints, which is entirely attributed to the change of the microstructure and the interface migration occurring during homogenization. The interface migration is driven by the interface curvature between two dissimilar IMC layers, strongly depending on bonding temperature. As a result, the micro-topography of the wave-shaped $\text{Cu}_6\text{Sn}_5/\text{Ag}_3\text{Sn}$ interface is extremely “smooth”, while that of the planar $\text{Cu}_3\text{Sn}/\text{Ag}_3\text{Sn}$ interface is quite “rough”.
- (2) Coating a thin Cu film on the Ag substrate to introduce the second phase of Cu_6Sn_5 particles can eliminate the shrinkage pores as well, because these particles efficiently fill the micropores distributing along Ag_3Sn grain boundaries. A critical thickness of the Cu film was proposed to determine the distribution shape of Cu_6Sn_5 IMCs: dispersive particles or continuous layer. This critical value can be determined by the required Cu film that allows most of the gaps between neighboring Cu_6Sn_5 grains to be closed. In addition, the Cu film should not be excessively thin ($<0.5\ \mu\text{m}$), otherwise micropores will remain in the IMC layer.
- (3) Both novel methods have been experimentally verified to improve the mechanical properties

of TLP joints. Shear strength of “Cu/Sn/Ag” was determined with a highest value of more than 48 MPa, and that of “Ag (Cu)/Sn/Ag” exceeded 40 MPa. They are greater than that of “Ag/Sn/Ag” which is approximately 31 MPa. The compact microstructures observed from the fracture surfaces demonstrate the valid elimination of pores by the introduction of Cu–Sn IMCs.

Acknowledgements

This work was financially supported by the National Science Foundation of China under Grant No. 51375260, which is entitled “Technology and Mechanism of Low Temperature Transient Liquid Phase Bonding”.

Compliance with ethical standards

Conflict of interest The authors declare that they have no conflict of interest.

References

- [1] Manikam VR, Cheong KY (2002) Die attach materials for high temperature applications: a review. *IEEE Trans Compon Packag Manuf Technol* 1:457–478
- [2] Neudeck PG, Okojie RS, Chen L (2002) High-temperature electronics—a role for wide bandgap semiconductors. *Proc IEEE* 90:1065–1076
- [3] Cook GO, Sorensen CD (2011) Overview of transient liquid phase and partial transient liquid phase bonding. *J Mater Sci* 46:5305–5323. doi:10.1007/s10853-011-5561-1
- [4] Li JF, Agyakwa PA, Johnson CM (2011) Interfacial reaction in Cu/Sn/Cu system during the transient liquid phase soldering process. *Acta Mater* 59:1198–1211
- [5] Chu K, Sohn Y, Moon C (2015) A comparative study of Cu/Sn/Cu and Ni/Sn/Ni solder joints for low temperature stable transient liquid phase bonding. *Scr Mater* 109:113–117
- [6] Tollefsen TA, Larsson A, Løvvik OM, Aasmundtveit K (2012) Au–Sn SLID bonding—properties and possibilities. *Metall Mater Trans B* 43:397–405
- [7] Li JF, Agyakwa PA, Johnson CM (2010) Kinetics of Ag_3Sn growth in Ag–Sn–Ag system during transient liquid phase soldering process. *Acta Mater* 58:3429–3443
- [8] Liu J, Kumar P, Dutta I, Raj R, Sidhu R, Renavikar M, Mahajan R (2011) Liquid phase sintered Cu–In composite

- solders for thermal interface material and interconnect applications. *J Mater Sci* 46:7012–7025. doi:[10.1007/s10853-011-5670-x](https://doi.org/10.1007/s10853-011-5670-x)
- [9] Bosco NS, Zok FW (2004) Critical interlayer thickness for transient liquid phase bonding in the Cu-Sn system. *Acta Mater* 52:2965–2972
- [10] Wang PJ, Sha CH, Lee CC (2010) Silver microstructure control for fluxless bonding success using Ag-In system. *IEEE Trans Compon Packag Technol* 33:462–469
- [11] Lis A, Leinenbach C (2015) Effect of process and service conditions on TLP-bonded components with (Ag, Ni)-Sn interlayer combinations. *J Electron Mater* 44:4576–4588
- [12] Liu H, Wang K, Aasmundtveit KE, Hoivik N (2012) Intermetallic compound formation mechanisms for Cu-Sn solid-liquid interdiffusion bonding. *J Electron Mater* 41:2453–2462
- [13] Kim JY, Yu J (2008) Effects of residual impurities in electroplated Cu on the Kirkendall void formation during soldering. *Appl Phys Lett* 92:92109–92112
- [14] Yu C, Chen J, Cheng Z, Huang Y, Chen J, Xu J, Lu H (2016) Fine grained Cu film promoting Kirkendall voiding at Cu₃Sn/Cu interface. *J Alloy Compd* 660:80–84
- [15] Yin L, Borgesen P (2011) On the root cause of Kirkendall voiding in Cu₃Sn. *J Mater Res* 26:455–466
- [16] Kim SH, Yu J (2013) Heat-treatment to suppress the formation of Kirkendall voids in Sn-3.5Ag/Cu solder joints. *Mater Lett* 106:75–78
- [17] Chang Y, Hsieh Y, Chen K (2014) Submicron Cu/Sn bonding technology with transient Ni diffusion buffer layer for 3DIC application. *IEEE Electron Device Lett* 35:1118–1120
- [18] Chia PY, Haseeb ASMA (2015) Intermixing reactions in electrodeposited Cu/Sn and Cu/Ni/Sn multilayer interconnects during room temperature and high temperature aging. *J Mater Sci* 26:294–299. doi:[10.1007/s10854-014-2398-9](https://doi.org/10.1007/s10854-014-2398-9)
- [19] Chidambaram V, Bangtao C, Lip GC, Woo DRM (2014) Au-In-based hermetic sealing for MEMS packaging for down-hole application. *J Electron Mater* 43:2498–2509
- [20] Chu K, Sohn Y, Moon C (2015) A comparative study of Cu/Sn/Cu and Ni/Sn/Ni solder joints for low temperature stable transient liquid phase bonding. *Scr Mater* 109:113–117
- [21] Shao H, Wu A, Bao Y, Zhao Y, Zou G (2016) Microstructure characterization and mechanical behavior for Ag₃Sn joint produced by foil-based TLP bonding in air atmosphere. *Mater Sci Eng A*. doi:[10.1016/j.msea.2016.10.092](https://doi.org/10.1016/j.msea.2016.10.092)
- [22] Shao H, Wu A, Bao Y, Zhao Y, Zou G (2016) Interfacial reaction and mechanical properties for Cu/Sn/Ag system low temperature transient liquid phase bonding. *J Mater Sci* 27:4839–4848. doi:[10.1007/s10854-016-4366-z](https://doi.org/10.1007/s10854-016-4366-z)
- [23] Yu H, Sun Y, Alpay SP, Aindow M (2016) Solidification microstructures in Ag₃Sn–Cu₃Sn pseudo-binary alloys. *J Mater Sci* 51:6474–6487. doi:[10.1007/s10853-016-9947-y](https://doi.org/10.1007/s10853-016-9947-y)
- [24] Baker OH (1992) ASM handbook: alloy phase diagrams version 3. ASM International, Metals Park
- [25] Hang C, Tian Y, Zhang R, Yang D (2013) Phase transformation and grain orientation of Cu-Sn intermetallic compounds during low temperature bonding process. *J Mater Sci* 24:3905–3913. doi:[10.1007/s10854-013-1337-5](https://doi.org/10.1007/s10854-013-1337-5)
- [26] Yuan Y, Guan Y, Li D, Moelans N (2016) Investigation of diffusion behavior in Cu-Sn solid state diffusion couples. *J Alloy Compd* 661:282–293
- [27] Ip SW, Toguri JM (1994) The equivalency of surface tension, surface energy and surface free energy. *J Mater Sci* 29:688–692. doi:[10.1007/BF00445980](https://doi.org/10.1007/BF00445980)
- [28] Upmanyu M, Smith RW, Srolovitz DJ (1998) Atomistic simulation of curvature driven grain boundary migration. *Interface Sci* 6:41–58
- [29] Farrer JK, Carter CB, Ravishankar N (2006) The effects of crystallography on grain-boundary migration in alumina. *J Mater Sci* 41:661–674. doi:[10.1007/s10853-006-6482-2](https://doi.org/10.1007/s10853-006-6482-2)
- [30] Chuang HY, Yu JJ, Kuo MS, Tong HM, Kao CR (2012) Elimination of voids in reactions between Ni and Sn: a novel effect of silver. *Scr Mater* 66:171–174
- [31] Chang J, Chang T, Chuang T, Lee C (2014) dual-phase intermetallic interconnection structure and method of fabricating the same. US Patent US9742600B2
- [32] Dybkov VI (1998) Growth kinetics of chemical compound layers. Cambridge International Science, Cambridge
- [33] Yoon J, Jung S (2008) Effect of immersion Ag surface finish on interfacial reaction and mechanical reliability of Sn-3.5Ag-0.7Cu solder joint. *J Alloy Compd* 458:200–207
- [34] Gagliano RA, Ghosh G, Fine ME (2002) Nucleation kinetics of Cu₆Sn₅ by reaction of molten tin with a copper substrate. *J Electron Mater* 31:1195–1202
- [35] Liu AA, Kim HK, Tu KN, Totta PA (1996) Spalling of Cu₆Sn₅ spheroids in the soldering reaction of eutectic SnPb on Cr/Cu/Au thin films. *J Appl Phys* 80:2774–2780